Efficiency of thermoelectric energy conversion in biphenyl-dithiol junctions: Effect of electron-phonon interactions

Nikolai Sergueev,[1,2] Seungha Shin,[2] Massoud Kaviany,[2] and Barry Dunietz[1,*]
[1]*Department of Chemistry, University of Michigan, Ann Arbor, Michigan 48109, USA*
[2]*Department of Mechanical Engineering, University of Michigan, Ann Arbor, Michigan 48109, USA*
(Received 3 November 2010; revised manuscript received 1 February 2011; published 9 May 2011)

The electron-phonon interaction is the dominant mechanism of inelastic scattering in molecular junctions. Here we report on its effect on the thermoelectric properties of single-molecule devices. Using density functional theory and the nonequilibrium Green's function formalism we calculate the thermoelectric figure of merit for a biphenyl-dithiol molecule between two Al electrodes under an applied gate voltage. We find that the effect of electron-phonon coupling on the thermoelectric characteristics strongly varies with the molecular geometry. Two molecular configurations characterized by the torsion angles between the two phenyl rings of 30° and 90° exhibit significantly different responses to the inelastic scattering. We also use molecular dynamics calculations to investigate the torsional stability of the biphenyl-dithiol molecule and the phonon thermal transport in the junction.

DOI: 10.1103/PhysRevB.83.195415 PACS number(s): 81.07.Nb, 68.37.Ef, 72.10.−d, 73.63.−b

I. INTRODUCTION

Charge and energy transport at the nanoscale is of current interest with implications in electronic, structural, and transport properties of electronic devices.[1–12] These also include applications based on the thermoelectric (TE) effect where thermal energy is converted into electrical energy. However, the TE effect has been mainly observed in bulk materials. Recent experiments[13–16] on atomic and molecular junctions have demonstrated that nanoscale devices can also exhibit a TE behavior. These experiments have inspired theoretical interest in predicting the TE properties of nanoscale junctions.[17–23] One of the key TE characteristics is the Seebeck coefficient, which measures the magnitude of the electric potential generated in response to a temperature gradient across the junction. The Seebeck coefficient is not only the key to the TE efficiency of the device. It also provides insight into the conductance mechanism. The overall efficiency of thermal-to-electric energy conversion is described by the dimensionless figure of merit (ZT) which depends on electrical and thermal conductance in addition to the Seebeck coefficient.

As in the bulk materials, the charge transport in molecular junctions is affected by the phonons. An electron interacts with phonons (molecular vibrations) and tunnel through the junction inelastically, i.e. loosing or gaining energy. The electron-phonon (e-p) interaction substantially alters the transmission probability and leads to various inelastic effects such as heat dissipation. The inelastic scattering and the effect of e-p interaction in molecular scale junctions have been studied extensively, both theoretically[5,24–28] and experimentally.[29–33] Despite the remarkable progress in theoretical modeling of TE junctions, most of the studies are based on the elastic description of the electron tunneling processes. Others use scattering theory approaches to treat phonons.[34,35] Recently Galperin *et al.*[17] reported on the strong effect of the e-p coupling on the calculation of the Seebeck coefficient using a self-consistent approach to treat molecular vibrations with a simple phenomenological model.

The purpose of this paper is to show the effect of inelastic scattering on the TE characteristics of molecular junctions (fully from first principles). This requires that in calculating the ZT figure of merit the Seebeck coefficient and electrical conductance are calculated with the e-p interaction included. We use an atomistic description of a molecular junction within density functional theory (DFT) and the nonequilibrium Greenâ's function (NEGF) formalism for both electron and phonon transport. Self-consistency is obtained between the electronic Hamiltonian and charge density under constant e-p coupling. Our junction model consists of a biphenyl-dithiol molecule sandwiched between two Al electrodes, as shown schematically in Fig. 1. Below, we show that the TE properties are greatly affected by electron inelastic scattering. We show that the qualitative effect of e-p interactions on transport depends strongly on the junction configuration.

The rest of the paper is organized as follows. We begin with a theoretical model, including the theory of inelastic scattering, thermoelectricity, and phonon propagation within the harmonic approximation. Each theory describes an important ingredient in evaluating a ZT factor. Section III contains the numerical results for the biphenyl-dithiol molecular junction and discusses the dependence of the TE properties on the e-p coupling, electron and phonon thermal transport, and the role of anharmonicity on the phonon conductivity. Section IV is a summary.

II. THEORETICAL MODEL

A. Electron transport within DFT-NEGF

We start by writing the total Hamiltonian of the molecular tunneling junction including the e-p interaction in the following form:

$$\hat{\mathrm{H}} = \hat{\mathrm{H}}_e + \hat{\mathrm{H}}_p + \hat{\mathrm{H}}_{e-p}, \tag{1}$$

where $\hat{\mathrm{H}}_e$ is the electronic contribution represented by the Kohn-Sham (KS) Hamiltonian. $\hat{\mathrm{H}}_p$ is the phonon Hamiltonian which is written within the second quantization as

$$\hat{\mathrm{H}}_p = \sum_\nu \hbar\omega_\nu \left(\hat{b}_\nu^\dagger \hat{b}_\nu + \frac{1}{2}\right), \tag{2}$$

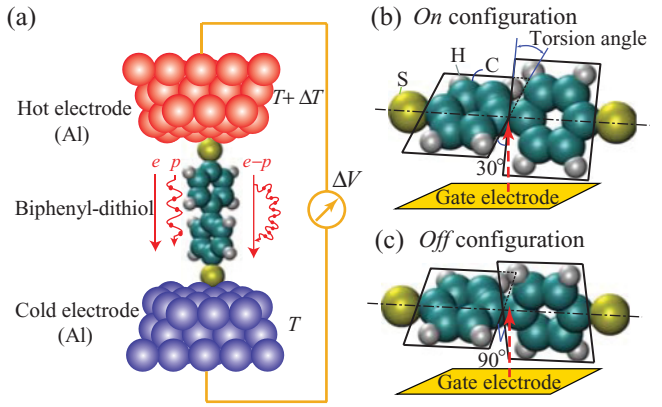

FIG. 1. (Color online) (a) The biphenyl-dithiol molecule between two Al electrodes and the electron and phonon energy carriers and their coupling. The molecular *on* (b) and *off* (c) states are characterized by the torsion angles (angle between the planes of the phenyl rings) of 30° and 90°, respectively.

where $\hat{b}_\nu^\dagger$ ($\hat{b}_\nu$) is the creation (annihilation) operator of the molecular vibrational mode ν. By "phonons" we refer to quantized molecular vibrations in the junction region. The last part of Eq. (1), $\hat{\mathrm{H}}_{e-p}$, represents the interaction of electrons with phonons in the junction region and is calculated as

$$\hat{\mathrm{H}}_{e-p} = \sum_\nu \sum_{ij} \mathbf{M}_{ij}^\nu |\phi_i\rangle\langle\phi_j|(\hat{b}_\nu^\dagger + \hat{b}_\nu). \tag{3}$$

Here the *e-p* coupling matrix $\mathbf{M}^\nu$ is expressed using localized atomic orbital (LCAO) basis functions ($|\phi_i\rangle$) as

$$\mathbf{M}_{ij}^\nu = \sum_\alpha \left(\frac{\hbar}{2m_\alpha\omega_\nu}\right)^{1/2} \mathbf{e}_\alpha^\nu \langle\phi_i|\frac{\partial \hat{\mathrm{H}}_e}{\partial \mathbf{R}_\alpha}|\phi_j\rangle, \tag{4}$$

where $\mathbf{e}^\nu$ and ω_ν are the eigenvectors and eigenfrequencies of the dynamical matrix $\mathbf{K}$,

$$\mathbf{K} = \{\mathbf{K}_{\alpha\beta}\} = (m_\alpha m_\beta)^{-1/2} \frac{\partial^2 E_{\mathrm{tot}}}{\partial \mathbf{R}_\alpha \partial \mathbf{R}_\beta}. \tag{5}$$

The quantum transport is well represented in the space of the eigenvectors projected onto the junction model region. The bridging region includes the six outermost surface layers of the functionalized surface with a molecular bridge as described in detail below.

Once the total Hamiltonian is defined, we describe many-body effects using the Green's functions. In the case where no *e-p* interactions are considered (i.e., the *e-p* coupling matrix M^ν is zero for all the vibrational modes) the electrons and phonons can be treated separately. In this limit, the bare retarded electron Green's function becomes

$$\mathbf{G}_0^R(E) = \left[E\mathbf{S} - \mathbf{H}_{KS} - \mathbf{\Sigma}_L^R(E) - \mathbf{\Sigma}_R^R(E)\right]^{-1}. \tag{6}$$

Here $\mathbf{\Sigma}_{L/R}^R$ is the retarded self-energy that describes interaction of the scattering region with the left/right (*L*/*R*) electrode. Under nonequilibrium effects resulting from an applied bias, the lesser nonequilibrium electron Green's functions are evaluated using

$$\mathbf{G}_0^<(E) = i\mathbf{G}_0^R(E)[\mathbf{\Sigma}_L^<(E) + \mathbf{\Sigma}_R^<(E)]\mathbf{G}_0^A(E). \tag{7}$$

Here $\mathbf{G}_0^A = (\mathbf{G}_0^R)^\dagger$ is the bare advanced electron Green's function. The bias-driven electron injection into the junction region is represented by the $\mathbf{\Sigma}_{L/R}^<$ as

$$\begin{aligned}\mathbf{\Sigma}_{L/R}^<(E,\mu_{L/R}) &= i f_{L/R}(E,\mu_{L/R})\mathbf{\Gamma}_{L/R}(E) \\ &= -f_{L/R}(E,\mu_{L/R})\left[\mathbf{\Sigma}_{L/R}^R(E) - \mathbf{\Sigma}_{L/R}^A(E)\right].\end{aligned} \tag{8}$$

In the last expression we denote by $f_{L/R}$ the Fermi distribution function of the left/right electrode shifted by the chemical potential $\mu_{L/R}$ and by $\mathbf{\Gamma}_{L/R}$ the electrode broadening functions. The lesser Green's function then also depends on the chemical potentials. In what follows we may omit the notations for the chemical potentials and for the electron energy for simplicity when needed.

Having defined the electronic Green's functions, we next consider the bare phonon ones. In what follows we assume an infinite lifetime of phonons, i.e., the characteristic time scale of electronic processes is much smaller than that of phonon processes. Electrons repeatedly scatter off the phonons before undergoing any energy changes. Within this approximation the bare retarded and nonequilibrium Green's functions of the phonon with the frequency ω_ν are defined as

$$\mathbf{D}_{0,\nu}^R(\Omega) = \frac{1}{\Omega - \hbar\omega_\nu + i\eta} - \frac{1}{\Omega + \hbar\omega_\nu + i\eta} \tag{9}$$

and

$$\begin{aligned}\mathbf{D}_{0,\nu}^<(\Omega) = -2\pi i[&(N_\nu + 1)\delta(\Omega + \hbar\omega_\nu) \\ &+ N_\nu\delta(\Omega - \hbar\omega_\nu)],\end{aligned} \tag{10}$$

where N_ν is the phonon occupation number, $\delta(\Omega \pm \hbar\omega_\nu)$ is the Dirac delta function, and η is an infinitesimally small real number. In this paper we also assume an equilibrium phonon distribution, i.e., the phonon occupation number is given by the Bose-Einstein distribution function $N_\nu = n_B(\omega_\nu)$.

We now consider the effect of *e-p* interaction on the electronic system. In the presence of *e-p* interaction we solve the many-body problem perturbatively, i.e., the electron Green's functions are corrected by self-energies representing the *e-p* coupling. We use the lowest-order Feynman diagrams and the Langreth rules for analytical continuation to calculate the *e-p* self-energies.[36] In this approach, both the retarded and the nonequilibrium self-energies for the electron Green's function corresponding to the Fock diagram are written as

$$\begin{aligned}\mathbf{\Sigma}_{e-p}^R(E) = i\hbar \sum_\nu \int \frac{d\Omega}{2\pi} \mathbf{M}^\nu \big[&\mathbf{G}_0^<(E-\Omega)\mathbf{D}_{0,\nu}^R(\Omega) \\ &+ \mathbf{G}_0^R(E-\Omega)\mathbf{D}_{0,\nu}^R(\Omega) + \mathbf{G}_0^R(E-\Omega)\mathbf{D}_{0,\nu}^<(\Omega)\big]\mathbf{M}^\nu\end{aligned} \tag{11}$$

$$\mathbf{\Sigma}_{e-p}^<(E) = i\hbar \sum_\nu \int \frac{d\Omega}{2\pi} \mathbf{M}^\nu \mathbf{G}_0^<(E-\Omega)\mathbf{D}_{0,\nu}^<(\Omega)\mathbf{M}^\nu. \tag{12}$$

In this paper we neglect the self-energy contribution due to the Hartree diagram as it is frequency independent and thus constant.[36] In fact, it is often omitted, as, e.g., in approaches based on the self-consistent Born approximation (SCBA).[26,37–40] Such a contribution is expected to renormalize the electron transmission function, leaving its derivative

intact.[41] Given the e-p interaction self-energies, the electron Green's functions are written as

$$\mathbf{G}^R(E) = \left[E\mathbf{S} - \mathbf{H}_{KS} - \mathbf{\Sigma}_L^R(E) - \mathbf{\Sigma}_R^R(E) - \mathbf{\Sigma}_{e-p}^R(E)\right]^{-1} \tag{13}$$

and

$$\mathbf{G}^<(E) = \mathbf{G}^R(E)\left[\mathbf{\Sigma}_L^<(E) + \mathbf{\Sigma}_R^<(E) + \mathbf{\Sigma}_{e-p}^<(E)\right]\mathbf{G}^A(E). \tag{14}$$

As described above, the electrodes' and e-p coupling effects on the electronic density are represented by the self-energy expressions in the corresponding Green's functions expressions. This requires that the perturbative treatment considers the self-consistency between the self-energies and the calculated Green's functions. While the e-p self-energies are obtained using the electronic Green's functions [see Eqs. (11) and (13)] we restrict our treatment to the linear term in the expansion over the e-p self-energies, namely, the e-p self-energies are kept constant. An update of the e-p self-energies is required to guarantee current conservation and is invoked, for example, in the SCBA approaches.[26,38,40] The self-consistent treatment of the self-energies is, however, rather involved and beyond the scope of this work. The remaining self-consistent aspect, and in our opinion also the more important, is the relationship between the Green's function and the perturbed electronic charge density under the effect of bulk coupling. In the implemented DFT-NEGF combined formalisms, the electronic Hamiltonian is a functional of the electron density extracted from the nonequilibrium Green's functions,[36,42–44]

$$\hat{\rho} = -\frac{1}{2\pi}\int dE\, \mathbf{G}^<(E). \tag{15}$$

Therefore, we compute the e-p self-energies [see Eqs. (11) and (12)] using the bare unperturbed electron Green's functions and enforce the self-consistency between the biased charge density and the Green's functions.

In DFT-NEGF the density matrix and the electronic Hamiltonian are self-consistently iterated under the effect of coupling to the voltage-biased electrodes. In this scheme the self-consistency accounts for the nonequilibrium statistics of the injected electrons. Once the iterative solution is obtained, the transport properties of the tunneling junction are then obtained from the fully responded electronic density. The electron current flowing into the scattering region from, e.g., the left electrode can be generally written in terms of the Green's functions as[36,45]

$$J = \frac{2e}{h}\int dE\, \mathrm{Tr}[\mathbf{\Sigma}_L^<(E)\mathbf{G}^>(E) - \mathbf{\Sigma}_L^>(E)\mathbf{G}^<(E)]. \tag{16}$$

The electron current can also be written in terms of the transmission function as

$$J = \frac{2e}{h}\int dE\, \mathcal{T}_e(E,V_b)[f_L(E,\mu_L) - f_R(E,\mu_R)], \tag{17}$$

where V_b is the bias applied across the junction, defined as $\mu_L - \mu_R$. The transmission function $\mathcal{T}_e$ can be written as a sum of elastic and inelastic components,

$$\mathcal{T}_e = \mathcal{T}_e^{\mathrm{el}} + \mathcal{T}_e^{\mathrm{inel}}. \tag{18}$$

The elastic component is given by the following relation:[46]

$$\mathcal{T}_e^{\mathrm{el}} = \mathrm{Tr}[\mathbf{\Gamma}_L\mathbf{G}^R\mathbf{\Gamma}_R\mathbf{G}^A], \tag{19}$$

where $\mathbf{\Gamma}_{L/R}$ is the broadening function due to the interaction of the scattering region with the left/right electrode. The inelastic contribution to the transmission function is written similarly as

$$\mathcal{T}_e^{\mathrm{inel}} = \mathrm{Tr}[\mathbf{\Gamma}_L\mathbf{G}^R\mathbf{\Gamma}_{e-p,R}\mathbf{G}^A]. \tag{20}$$

The $\mathbf{\Gamma}_{e-p}$ is the total broadening function due to the e-p interaction and can be expressed as a sum of two contact terms $\mathbf{\Gamma}_{e-p} = \mathbf{\Gamma}_{e-p,L} + \mathbf{\Gamma}_{e-p,R}$.[47]

B. Calculation of the thermoelectric figure of merit

The efficiency of the TE energy conversion is usually described by the dimensionless quantity called the TE figure of merit (ZT), which is defined as

$$ZT = \frac{S^2 G_e}{G_{t,e} + G_{t,p}}T, \tag{21}$$

where S is the Seebeck coefficient describing magnitude of the TE voltage induced by the temperature difference across the tunneling junction, G_e is the electrical conductance, and $G_{t,e}$ and $G_{t,p}$ are the thermal conductances due to electrons and phonons, respectively. T is the temperature at the absolute scale.

In order to calculate the TE figure of merit let us first write the electric J and thermal Q currents in the junction as

$$J = \frac{2e}{h}\int_{-\infty}^{\infty} dE\, \mathcal{T}_e[f_L - f_R], \tag{22}$$

$$Q = Q_e + Q_p = \frac{2}{h}\int_{-\infty}^{\infty} dE\,(E - E_f)\,\mathcal{T}_e[f_L - f_R] + \frac{\hbar}{2\pi}\int_0^{\infty} d\omega\,\omega\,\mathcal{T}_p[n_L - n_R], \tag{23}$$

where E_f is the Fermi energy defined by the external electrodes, $\mathcal{T}_e$ and $\mathcal{T}_p$ are the electron and phonon transmission functions, respectively, and $n_{L/R}$ is the Bose-Einstein distribution function for the left/right electrode. In what follows we focus on the electron thermal current Q_e which is the first part of Eq. (23), leaving the discussion of the phonon thermal current for the next subsection. As the junction TE formalism is based on the linear expansion approach (as discussed later), the electrical thermal current in Eq. (23) is calculated in the limit of vanishing temperature differences. Thus the Fermi energy here is defined as an average of the electrochemical potentials of the two electrodes.

The thermopower of the tunneling junction, given by the Seebeck coefficient, measures the induced TE voltage built up in response to the temperature difference applied across the junction. If the temperature difference between the two ends of the junction is small, then the Seebeck coefficient is defined as

$$S = -\frac{\Delta V}{\Delta T}, \tag{24}$$

where ΔV is the TE voltage difference between the electrodes generated in response to the temperature difference ΔT across

the tunneling junction. The electric current is linearly expanded in terms of the voltage and temperature differences across the junction,[17]

$$J = \frac{\partial J}{\partial(\Delta V)}\Delta V + \frac{\partial J}{\partial(\Delta T)}\Delta T = G_e \Delta V + L\Delta T. \quad (25)$$

Therefore, the Seebeck coefficient at the limit of zero current is rewritten as

$$S = \frac{L}{G_e}. \quad (26)$$

Here G_e is the electrical conductance while L can be referred as the electrical thermal coefficient.

In a similar fashion the electron thermal conductance can be obtained. Expansion of the thermal current yields the following:

$$Q_e = \frac{\partial Q_e}{\partial(\Delta V)}\Delta V + \frac{\partial Q_e}{\partial(\Delta T)}\Delta T = R\Delta V + F\Delta T. \quad (27)$$

Then the electron thermal conductance can be written as

$$G_{t,e} = \frac{Q_e}{\Delta T} = R\frac{\Delta V}{\Delta T} + F = -R\,S + F. \quad (28)$$

In the Landauer approximation the Seebeck coefficient and the electron thermal conductance can take the following form:[18]

$$S = \frac{K_1}{eK_0}, \quad (29)$$

where K_n is defined as

$$K_n = \frac{2}{h}\int_{-\infty}^{\infty} dE\, \mathcal{T}_e(E)\left(-\frac{\partial f_L}{\partial E}\right)(E - E_f)^n. \quad (30)$$

In the zero-voltage- and zero-temperature-bias limits, the electron thermal conductance becomes

$$G_{t,e} = \left(K_2 - \frac{K_1^2}{K_0}\right)\frac{1}{T}. \quad (31)$$

We, therefore, calculate both the Seebeck coefficient and the electron thermal conductance via the more general formulation of Eqs. (26) and (28), respectively, to address the *e-p* interaction.

At this modeling level, the Seebeck coefficient is obtained by first calculating the TE current $J(\Delta T)$ induced by the temperature difference ΔT (at $\Delta V = 0$). We then apply the voltage ΔV (at $\Delta T = 0$) that generates the same tunneling current, i.e., $J(\Delta T) = J(\Delta V)$. Division of the voltage difference by the temperature difference yields the Seebeck coefficient. In order to obtain the electron thermal conductance we first calculate the coefficients R and F in Eq. (28) by taking a numerical derivative of the electron thermal current Q_e with respect to the voltage ΔV and temperature ΔT differences, respectively. Use of R, F, and the Seebeck coefficient in Eq. (28) yields the electron thermal conductance.

C. Phonon transport within the NEGF formalism

We extend the NEGF formalism to treat phonon transport in molecular scale junctions.[7,48,49] A similar scheme as implemented for electron transport can be used here, where Bose-Einstein statistics is used for the phonons instead of the Fermi-Dirac statistics relevant for the electrons.[36] We start by calculating the dynamical matrix defined in the previous subsections by Eq. (5). As in the electron transport problem, the junction is divided into the central region and the left and right electrodes. The dynamical matrix of the junction then has the form

$$\mathbf{K} = \begin{bmatrix} \mathbf{K_{LL}} & \mathbf{K}_{LC} & 0 \\ \mathbf{K}_{CL} & \mathbf{K}_{CC} & \mathbf{K}_{CR} \\ 0 & \mathbf{K}_{RC} & \mathbf{K}_{RR} \end{bmatrix}. \quad (32)$$

Here $\mathbf{K}_{LL}$ and $\mathbf{K}_{RR}$ are the dynamical matrices of the semi-infinite left and right electrodes, respectively. Each electrode is defined as a set of layers periodically repeated in the transport direction with the interaction of only the nearest-neighboring layers. Then, for example, the left semi-infinite electrode dynamical matrix has the following form:

$$\mathbf{K}_{LL} = \begin{bmatrix} \ddots & \ddots & \ddots & \\ & \mathbf{K}_{l,l-1} & \mathbf{K}_{l,l} & \mathbf{K}_{l,l+1} \\ & 0 & \mathbf{K}_{l,l-1} & \mathbf{K}_{l,l} \end{bmatrix}, \quad (33)$$

where $\mathbf{K}_{l,l}$ is the dynamical matrix of the layer with index l while $\mathbf{K}_{l,l+1}$ or $\mathbf{K}_{l,l-1}$ describe interaction of the layer l with neighboring layers $l+1$ and $l-1$. The dynamical matrix of the right semi-infinite electrode is written in a similar fashion.

The central region is further partitioned into the scattering region and the regions representing the bulk left and right electrodes. The models representing the bulk regions are chosen to be large enough to effectively screen any effect of the molecule. The dynamical matrix of the central region is then written as

$$\mathbf{K}_{CC} = \begin{bmatrix} \mathbf{K_{l,l}} & \mathbf{K}_{l,c} & 0 \\ \mathbf{K}_{c,l} & \mathbf{K}_{c,c} & \mathbf{K}_{c,r} \\ 0 & \mathbf{K}_{r,c} & \mathbf{K}_{r,r} \end{bmatrix}, \quad (34)$$

where $\mathbf{K}_{l,l}$ and $\mathbf{K}_{r,r}$ are the dynamical matrices of the finite left and right electrodes, $\mathbf{K}_{c,c}$ is the dynamical matrix of the scattering region, and $\mathbf{K}_{l,c}$ and $\mathbf{K}_{r,c}$ are the interaction matrix elements. Finally, the matrices $\mathbf{K}_{LC}$ and $\mathbf{K}_{RC}$ describe interaction of the central region with the semi-infinite electrodes, where the only nonvanishing terms are due to nearest-neighbor interactions ($\mathbf{K}_{LC} = \mathbf{K}_{l,l+1}$ and $\mathbf{K}_{RC} = \mathbf{K}_{r,r+1}$).

The semi-infinite nature of the electrode, as in the electron transport system, is represented by phonon self-energies ($\mathbf{\Pi}_{L/R}$). The phonon Green's function of the central region connected to the semi-infinite electrodes is then written as

$$\mathbf{D}^R(\omega) = \left[\omega^2\mathbf{I} - \mathbf{K}_{CC} - \mathbf{\Pi}_L^R(\omega) - \mathbf{\Pi}_R^R(\omega)\right], \quad (35)$$

where $\mathbf{\Pi}_L^R(\omega)$ and $\mathbf{\Pi}_R^R(\omega)$ are the phonon retarded self-energies due to the interaction of the central region with the left and right electrodes, respectively.

To obtain the phonon self-energies we employ the iterative method proposed by Sancho *et al.*,[50] where the surface and bulk Green's functions are calculated iteratively and separately. Within this approach the self-energies and the surface Green's functions are obtained via the transfer matrices. We refer to Ref. 50 for more details.

Provided with the phonon retarded Green's functions of the scattering region, the phonon transport properties of the

junction can be calculated. The phonon thermal current is then given by

$$Q_p = \frac{\hbar}{2\pi}\int_0^\infty d\omega\,\omega\mathcal{T}_p(\omega)[n_L(\omega,T_L) - n_R(\omega,T_R)], \quad (36)$$

where $T_{L/R}$ is the temperature of the left/right electrode and the phonon transmission function $\mathcal{T}_p(\omega)$ is obtained as

$$\mathcal{T}_p(\omega) = Tr[\mathbf{\Omega}_L(\omega)\mathbf{D}^{\mathbf{R}}(\omega)\mathbf{\Omega}_R(\omega)\mathbf{D}^{\mathbf{A}}(\omega)]. \quad (37)$$

Here $\mathbf{D}^{\mathbf{A}} = (\mathbf{D}^{\mathbf{R}})^\dagger$ is the advanced phonon Green's function, and $\mathbf{\Omega}_{L/R}$ is the broadening function due to the interaction of the central region with left/right electrode defined as

$$\mathbf{\Omega}_{L/R}(\omega) = i\left[\mathbf{\Pi}^R_{L/R}(\omega) - \mathbf{\Pi}^A_{L/R}(\omega)\right]. \quad (38)$$

The phonon thermal conductance is then written as

$$G_{t,p} = \frac{Q_p}{\Delta T}, \quad (39)$$

where ΔT is defined as the difference between the temperatures of the left, T_L, and right, T_R, electrodes. In this paper the phonon thermal conductance is computed directly by taking a numerical derivative of the phonon thermal current with respect to the temperature difference.

III. RESULTS AND DISCUSSION

We investigate the effect of *e-p* coupling on the TE properties of a molecular junction by calculating its Seebeck coefficient, electrical and thermal conductances, and the TE figure of merit in the presence of the *e-p* interaction. As a model for a molecular bridge we couple a biphenyl-dithiol molecule to two Al(111) electrodes and apply a temperature and voltage gradient across the junction, as shown in Fig. 1(a). The scattering region of the junction includes the molecule and some portion of Al(111) electrodes of finite cross section (about 12.2 Å) at each side of the junction. Each such portion has three (4×4) layers of Al atoms. We perform a periodic calculation of the external electrodes, where k sampling is evoked only along the transport axis due to the finite cross section of the electrode models. The molecule is bound to the Al surface at the hollow sites. The calculated binding energy of the molecule to the Al electrodes is 2.37 eV which is larger than that for gold electrodes as reported.[51]

The dynamical matrices and vibrational spectrum are obtained at the DFT level using the SIESTA package.[52] Here we use the Troullier-Martins (TM) norm-conserving nonlocal pseudopotentials to treat atomic cores, Ceperley-Alder functionals for the exchange-correlation energy, and single-ζ localized atomic orbitals (LCAO) basis functions. For the quantum-transport calculations we use our developed numerical package based on the DFT-NEGF approach, discussed in Sec. II. It utilizes the LCAO basis set and the TM pseudopotentials with the Perdew-Wang 1992 (PW92) exchange correlation functional.

A. Biphenyl-dithiol: Two distinct junction configurations

Recent studies of the transport and conformational properties of biphenyl-based molecular junctions, both theoretical[53,54] and experimental,[54,55] suggest that the conductance greatly depends on the torsion angle between the two phenyl rings. The conductance is high when the two phenyl rings are in the same plane and decreases drastically when the torsion angle increases. When the phenyl rings are in perpendicular planes, the conductance is at minimum. The origin of such conductance variations lies in the overlap between the carbon π orbitals of different phenyl rings. The greater overlap corresponds to higher tunneling probability. The biphenyl-based junction can then be assigned with two transport regimes characterized by the high and low conductance values. In what follows we address the effect of the *e-p* coupling on the junction in both regimes.

We start by first studying the conformational properties of the biphenyl-dithiol molecule in the junction. We follow the energy of the molecular junction, where one phenyl ring is rotated relative to the other. We find that the structural minimum is a compromise between the tendency for parallel alignment of the two phenyl π systems and the intramolecular repulsion due to hydrogen atoms. Indeed, the stable configuration features about 30° rotation angle between the two phenyl rings as shown schematically in Fig. 1(b). The configuration with the perpendicular orientation of the rings [see Fig. 1(c)] corresponds to the transition geometry along the related torsion angle coordinate. The energy barrier between the stable and transition configurations is about 0.3 eV. Below, we refer to the semiplanar configuration as the *on* state and to the perpendicular as the *off* state, reflecting their conductance properties as indeed confirmed by our modeling.

The two configurations are used to demonstrate the rich relationship of structure and TE at the molecular level. We emphasize that while the *off* configuration is energetically unstable as a transition state it serves as a model of possible stable molecular orientations of related junctions. The perpendicular orientation can be stabilized by enhancing the repulsive interactions between the rings using steric substituents.[56] For example, such substitutions were used experimentally to design a study of the conductance dependence on the angle in biphenyl-derived junctions.[56] In order to gauge the role of steric substituents we added two methyl groups to one of the molecule's phenyl rings and performed total energy and quantum-transport calculations. Our results show that indeed, the addition of methyl groups resulted in perpendicular alignment of the rings. Furthermore, we also confirmed that the transport and TE properties as evaluated for the *off* model structure are *very* similar to those of the dimethyl-substituted junction. In fact, the effect of the phonon-assisted tunneling on the electron transmission function was found to be even more pronounced for the molecule with steric groups. This indicates that the *off* structure can successfully represent the junction in its low-conducting state.

Therefore, in what follows we remove the substituents from the *off* model. This allows a focused analysis of the TE properties of two different related configurations. The two models also follow earlier studies on the effect of substituents on the conductance properties in similar junctions.[53] Below we analyze the effect of the *e-p* interaction on the TE properties, where the two configurations are used to sample the high- and low-conductance regimes of the junction. We demonstrate

that indeed inelastic scattering effects on the TE properties exhibit a diverse behavior depending on the configuration and the nature of the relevant vibrational mode.

B. Electronic structure and band alignment

We first describe the electronic structure of the biphenyl-dithiol junction in the absence of *e-p* interaction. We calculate the electronic projected density of states (PDOS) on the molecular biphenyl-dithiol space using

$$D_{e,m} = -\frac{1}{\pi}\mathrm{Im}\sum_{i,j\in M}\mathbf{S}_{ij}\mathbf{G}^{R}_{ij}. \tag{40}$$

Figure 2 shows the PDOS of the *on* and *off* molecular configurations. The PDOSs for both configurations exhibit two peaks around the Fermi energy. The peaks are associated with the highest occupied (HOMO) and lowest unoccupied (LUMO) biphenyl-dithiol molecular states. We observe that the peaks are split due to the hybridization of the molecular and Al orbitals. Overall the electronic structure is similar: the DFT HOMO-LUMO gap is about 3.5–3.9 eV while the LUMO state is closer to the Fermi energy of the junction. Therefore the electron transport is mediated mainly by the LUMO state. The work function for Al is relatively small at 4.2 eV, where the gold value, for example, is 5.1 eV. In the case of Au electrodes, we expect the HOMO state to be closer to the Fermi energy.

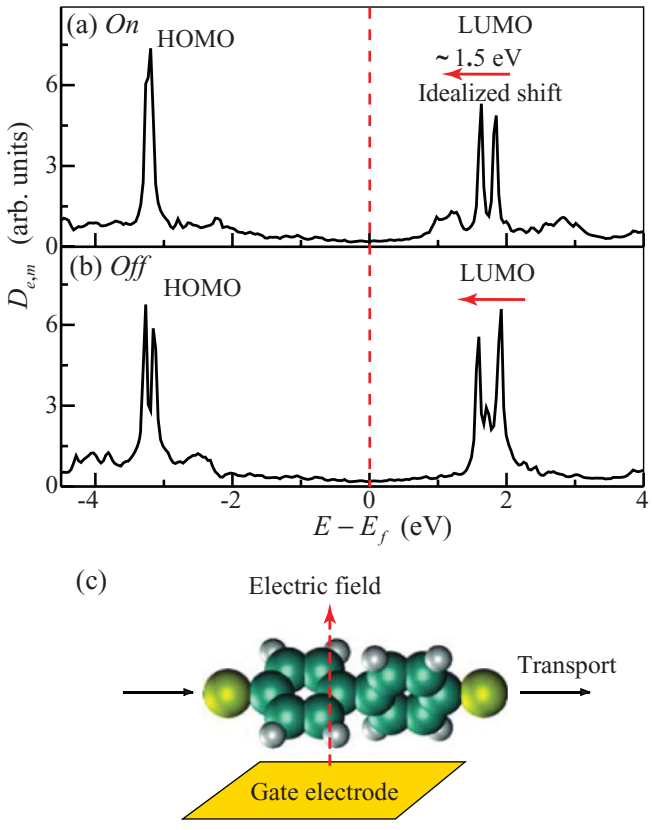

FIG. 2. (Color online) Electronic partial density of states of the biphenyl-dithiol molecule versus electron energy for the junction *on* (a) and *off* (b) states. The Fermi energy (indicated with the vertical dashed line) is shifted to zero. (c) Schematic of the junction with the applied gate electric field (shown with the red dashed arrow).

Gating the Al-contacted system moves the LUMO state and aligns it with the Fermi energy. This results in maximizing the Seebeck coefficient and the *e-p* effect. Indeed, the Seebeck coefficient is proportional to the derivative of the electronic density of states (DOS) with respect to energy at the Fermi level.[13] The same overall effect is found also when gating is not applied. We note that gating can be effected either by chemical substitution[57] or by adding a gating contact.[58–60] In this paper, we maximize the modeled Seebeck coefficient by applying a gating electric field, as shown in Fig. 2(c). We find that the electric field of about 1–1.5 V/Å effectively shifts the electronic states of the molecule. In the rest of the paper the TE properties of the junction are obtained under the effect of a fixed gating electric field of 1.2 eV/Å.

C. Inelastic electron scattering

We next incorporate the *e-p* coupling effect. We start by computing the vibrational spectrum of the biphenyl-dithiol molecule connected to the electrodes for both the *on* and *off* states. We obtain a dynamical matrix defined as the second derivative of the total energy with respect to atomic positions and diagonalize it to obtain its eigenfrequencies and eigenvectors. We include only real (nonimaginary) vibrational modes for computing the electron-phonon interaction and inelastic transport. We note that the *off* configuration, being a transition state, has one vibrational mode with imaginary frequency. The effect of the imaginary modes was confirmed to be negligible by comparing to relevant models with steric features that stabilize the twist angle between the two rings.

Having obtained the vibrational eigenmodes of the molecule we calculate the *e-p* coupling matrix using Eq. (4). The *e-p* coupling matrix is then included in the electronic Hamiltonian with the use of the self-energies as discussed in the previous section. The charge density of the device and the electron Green's functions with the self-energies representing the *e-p* effects are iterated until self-consistency is achieved. We then calculate the electron transmission function using Eq. (18).

Figure 3 shows the transmission function versus the tunneling electron energy for both the *on* and *off* states. We find that the effect of the *e-p* coupling on the electron transport for the *on* and *off* states is significantly different. When the junction is in the *on* state, adding the *e-p* interaction slightly diminishes the electron tunneling, as shown in Fig. 3(a). This effect is mainly due to the electrons coupling with the vibrational modes that stretch the phenyl rings. When the phenyl rings are in perpendicular planes, i.e., the junction is in the *off* state, the *e-p* interaction greatly enhances the electron transport. Such enhancement is mostly attributed to the phenyl rings' twisting mode. The rotation of the rings toward their parallel orientation creates a better overlap between the carbon π orbitals across the two rings. That is, the parallel orientation facilitates electron transport. All the other modes are found to be relatively inactive in affecting the transport.

We next study the effect of temperature on the electron transport in the junction.

Figure 4 shows the transmission function in the presence of the *e-p* interaction for both the *on* and *off* states. The increase in the junction temperature has no effect on the electron tunneling

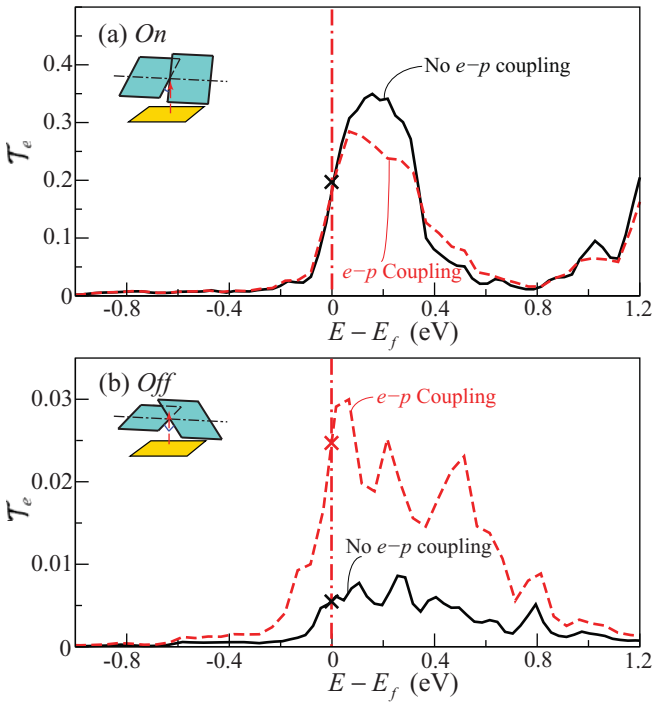

FIG. 3. (Color online) Electron transmission function of the biphenyl-dithiol TE junction versus energy for the *on* (a) and *off* (b) states with (dashed line) and without (solid line) *e-p* coupling.

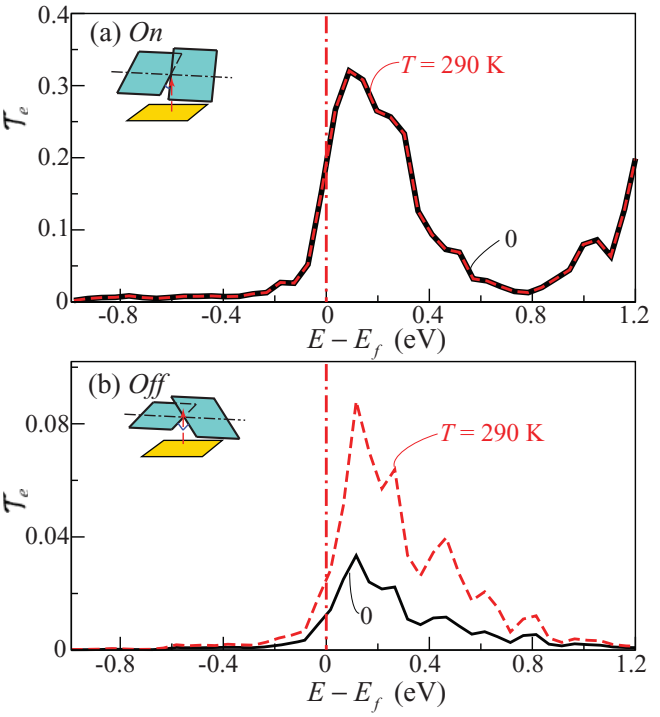

FIG. 4. (Color online) Electron transmission function of the biphenyl-dithiol TE junction versus energy for both the *on* (a) and *off* (b) states at junction temperatures of 0 (solid line) and 290 K (dashed line).

when the biphenyl-dithiol molecule is in the conductive state [see Fig. 4(a)]. However, when the molecule is in the *off* state, the increase in the junction temperature drastically enhances the transmission function. This is mainly due to the inelastic nature of the transport. As the temperature goes up, more and more vibrational modes become "activated" which effectively increases the number of inelastic tunneling channels. At the same time the junction in the *off* state is characterized by the lack of backscattering due to phonons, which could potentially reduce the electron transport.

The TE figure of merit depends on the electrical conductance of the junction. The latter is computed by taking the numerical derivative of the electric current with respect to the voltage difference. Figure 5 shows the electrical conductance of the junction as a function of the junction temperature for both the *on* and *off* states at zero bias voltage. The junction temperature is defined as the average of the two electrode temperatures. For both configurations the conductance does not change with the junction temperature when the *e-p* coupling is neglected. Indeed, at zero bias voltage, the conductance can be expressed in terms of the transmission function as $G_e = 2e^2\,\mathcal{T}_e(E = E_f)/h$. For the *on* state, the conductance is slightly shifted by the *e-p* coupling but overall does not depend also on the temperature. The *off* state conductance, on the other hand, is strongly enhanced by the *e-p* coupling and therefore depends strongly on the temperature.

We now evaluate the Seebeck coefficient using Eqs. (24) and (26) as follows. We first compute the electric current (J) induced by the temperature difference (ΔT) between two electrodes at zero voltage difference. Then we apply a voltage difference (ΔV) that produces the same current (J) at zero temperature difference. The ratio of the voltage difference to the temperature difference in the limit of infinitesimal tunneling current yields the Seebeck coefficient.

Figure 6 shows the Seebeck coefficient versus junction temperature plotted for both the *on* and *off* states with and without *e-p* interaction included. The effect of inelastic scattering on the Seebeck coefficient for the *on* state is quite moderate. Indeed, the transmission functions [see Fig. 4(a)]

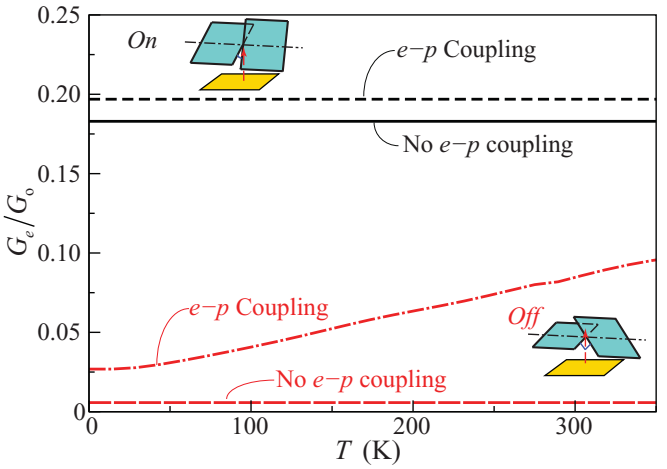

FIG. 5. (Color online) Electrical conductance of the biphenyl-dithiol TE junction versus junction temperature for both the *on* [with (solid line) and without (dashed line) *e-p* coupling] and *off* [with (long-dashed line) and without (dot-dashed line) *e-p* coupling] states.

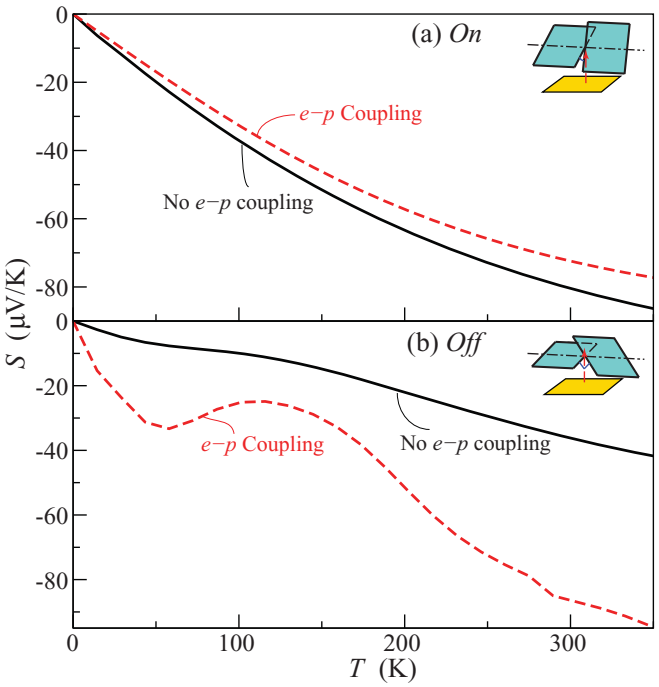

FIG. 6. (Color online) The Seebeck coefficient of the biphenyl-dithiol TE junction versus junction temperature for both the *on* (a) and *off* (b) states with (dashed line) and without (solid line) *e-p* coupling.

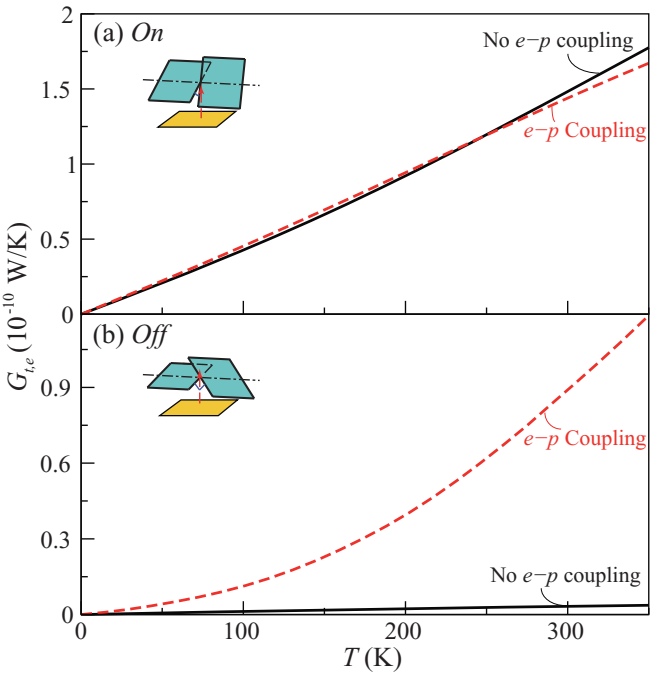

FIG. 7. (Color online) Electron thermal conductance of the biphenyl-dithiol TE junction versus junction temperature for the *on* (a) and *off* (b) states with and without *e-p* coupling.

indicate that the electron transport for this junction state is not sensitive to temperature variations. The effect of the *e-p* coupling for the *off* state is more pronounced, as shown in Fig. 6(b). In this case, the *e-p* interaction increases the Seebeck coefficient by a factor of roughly 2–4, since an increased temperature enhances the transmission function, as shown in Fig. 4(b). Therefore, a smaller temperature difference across the junction [which is in the denominator in Eq. (24)] is needed to generate the same electric current.

The calculated Seebeck coefficient for the *on* state at 300 K is about 60–70 μK/V. In this paper we use Al-based electrodes to bias the molecule. The applied gate potential leads to an enhanced Seebeck coefficient (as discussed in the previous subsection). The calculations of the TE properties are performed at the fixed positive gate electric field of 1.2 V/Å. Reddy *et al.*[13] report the Seebeck coefficient to be about 12 μV/K at room temperatures for the biphenyl-dithiol molecule in the junction between two Au electrodes. We note that our evaluated Seebeck coefficient is expected to be larger than that in a similar but not identical experiment.[13] Furthermore, the sign of the Seebeck coefficient is different because the transport is HOMO versus LUMO based.

Following the electrical conductance and the Seebeck coefficient of the biphenyl-dithiol junction, the next ingredient needed for the TE figure of merit is the electron thermal conductance, which is calculated using Eq. (28). Figure 7 shows the electron thermal conductance versus junction temperature of both the *on* and *off* states. Again we compare the results obtained with and without *e-p* coupling. As expected, the effect of the *e-p* coupling on the electron thermal conductance is negligible for the *on* state while it is substantial for the junction having phenyl rings in perpendicular relative orientation. For example, at $T = 250$ K, the electron thermal conductance obtained with the *e-p* interaction differs from that calculated using a pure elastic transport model by about a factor of 20. This change in the electron thermal conductance is crucial when computing the TE figure of merit since the phonon thermal conductance contribution remains relatively small (as shown in the next subsection).

D. Phonon conductivity of the biphenyl-dithiol junction

Finally, the last ingredient needed for the TE figure of merit is the thermal conductance due to phonons propagating through the junction. In order to calculate it we employ the elastic phonon transport method based on the Green's function formalism as discussed in Sec. II.

We start by computing the dynamical matrices of the left and right electrodes. Here we choose a bulk cell which is long enough in the phonon transport direction so that the *nearest-neighbor interaction approach* can be safely applied (see Sec. II for details). In our case the bulk cell has 3 (4×4) parallel layers of Al atoms. Having relaxed the atomic coordinates, we compute the matrices $\mathbf{K}_{l,l}$ and $\mathbf{K}_{l,l+1}$ and apply the iterative technique introduced by Sancho *et al.*[50] as described above to calculate the phonon surface Green's functions and the electrode phonon self-energies.

We next calculate the dynamical matrix of the central region. The central region contains the scattering region and the left and right bulk electrode cells. The scattering region should include not only the molecule but several layers of the electrodes. This guarantees that the molecule is effectively screened so that the left and right electrodes in the central region represent properly the bulk properties. In this work the scattering region contains a biphenyl-dithiol molecule

connected to 3 (4 × 4) layers of Al atoms on each of the left and right sides. We next compute the dynamical matrix $\mathbf{K}_{c,c}$ of the optimized central region model.

We calculate the phonon Green's function using Eq. (35), where the dynamical matrix of the central region is employed. The phonon transport properties represented by the phonon transmission function $\mathcal{T}_p$, phonon current Q_p, and phonon thermal conductance $G_{t,p}$ are computed following Eqs. (37), (36), and (39), respectively.

Figure 8 shows both the phonon transmission function and the phonon contribution to the thermal conductance versus junction temperature for the *on* and *off* states. We find that the phonon transport properties of the junction in the *on* state are very similar to those in the *off* state. The phonon thermal conductance is obtained by numerical differentiation of the phonon thermal current with respect to the temperature difference across the junction. As shown in Fig. 8(b), the phonon contribution to the thermal conductance of the biphenyl-dithiol junction is almost the same for both junction configurations. This similarity in the phonon thermal transport is in contrast to the variation of the electron thermal transport between the two configurations (see the electron thermal conductances compared in Fig. 7). Slight differences in phonon transport are noted with the enhancement of the transport in the *on* state by around 210 cm^{-1}. This is likely due to vibrational modes that involve stretching-squeezing motions of the phenyl rings. Such vibrations are less likely to be propagated through the junction with the phenyl rings in the perpendicular planes. We also plot the phonon thermal conductance normalized to the quantum of thermal conductance $G_{t,0} = \pi^2 k_B^2 T/3h$, as shown in Fig. 8(c). We find that the normalized phonon conductance of the biphenyl-dithiol TE junction reaches a maximum at a junction temperature of about 130 K.

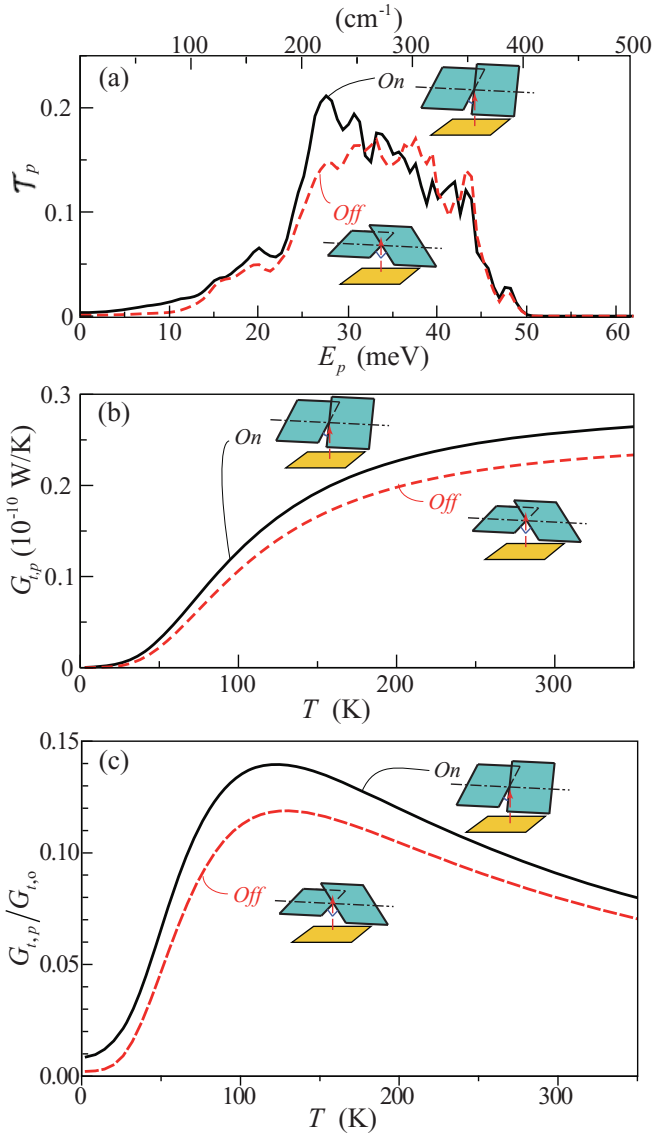

FIG. 8. (Color online) (a) Phonon transmission function of the biphenyl-dithiol TE junction, versus the frequency of the phonons for both the *on* and *off* states. (b) Phonon thermal conductance versus junction temperature for both the *on* and *off* states. (c) Phonon thermal conductance normalized by the quantum of thermal conductance versus junction temperature for both the *on* and *off* states.

E. Thermoelectric figure of merit

We calculate now the TE figure of merit following Eq. (21) using all the evaluated properties: the Seebeck coefficient (Fig. 6), the electrical conductance (Fig. 5), and the thermal conductances [Figs. 7 and 8(b)]. Figure 9 provides the TE figure of merit versus junction temperature for both *on* and *off* junction states. Similarly to effects on the Seebeck coefficient and electron thermal conductance, the effect of *e-p* coupling on the TE figure of merit is very moderate for the junction in the *on* state. For the junction in the *off* state the *e-p* coupling greatly enhances the TE figure of merit. For example, at

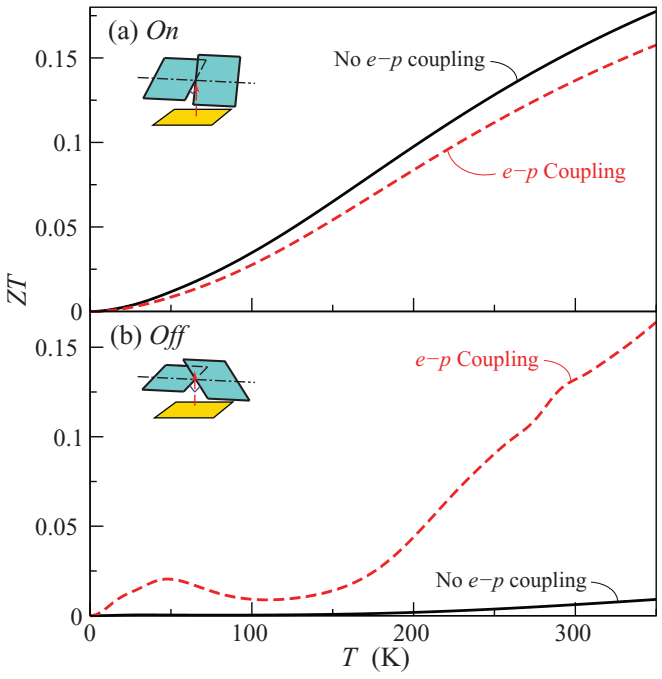

FIG. 9. (Color online) The TE figure of merit of the biphenyl-dithiol TE junction versus junction temperature for the *on* (a) and *off* (b) states with (dashed line) and without (solid line) *e-p* coupling.

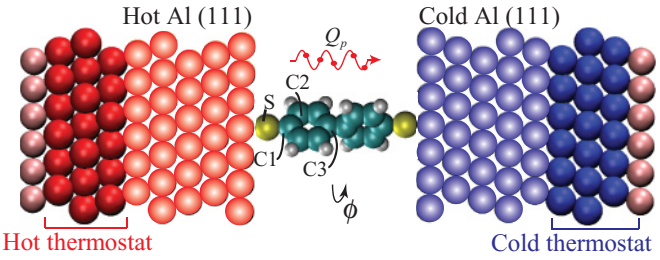

FIG. 10. (Color online) Atomic configuration used in MD simulations. The thermostat on each side is three Al layers and its temperature is controlled by the Langevin algorithm.

$T = 250$ K, taking into account the interaction of electrons and phonons leads to an increase in the figure of merit by about a factor of 20. Thus, for some junction geometries the e-p coupling has a great impact on the device's thermoelectric efficiency.

F. Torsion angle stability and anharmonicity investigated by molecular dynamics

Next we employ molecular dynamics (MD) simulations to investigate the stability with respect to the torsion angle and the phonon transport properties of the biphenyl-dithiol junction. Since the NEGF formalism for phonon transport employs dynamical matrices, the phonon conductance $G_{t,p}$ calculated above does not include anharmonicity. However, anharmonicity in phonon transport is omnipresent, especially at high temperatures. We calculate $G_{t,p}$ from the temperature distribution (ΔT) and heat flow (Q) in nonequilibrium MD (NEMD), where the temperature is controlled by the Langevin thermostat.[63] The NEMD simulations cover a temperature range of 280–500 K in the NVT ensemble (constant number of particles, volume, and temperature) with the hot ($T_{\rm hot}$) and cold ($T_{\rm cold}$) thermostat temperatures set 10% higher and 10% lower than the average temperature, respectively. The temperature gradient is large enough to mask the effects of temperature fluctuations.[64] In our model the biphenyl-dithiol molecule is sandwiched between two Al electrodes represented by 324 atoms each (see Fig. 10). We impose periodic boundary conditions in the lateral x and y directions for Al. The calculations run for 5 ns with 0.5 fs time steps. The interatomic potentials used in the molecular mechanics simulations are fitted against DFT calculations. Two-, three-, and four-body potentials are employed and are listed in Table I. Instead of direct inclusion of H atoms, the C-H groups are treated each as one entity (adding the mass of H to that of C).[61]

We invoke a quantum correction scheme to the MD simulations. The correction term takes the following form:[65–67]

$$k_B T_{\rm MD} = \int d\omega D_p(\omega)\hbar\omega \left(f_p^{\rm o} + \frac{1}{2}\right), \qquad G_{t,p} = G_{t,p,{\rm MD}} \frac{dT_{\rm MD}}{dT}. \tag{41}$$

Here $f_p^{\rm o}$ is the phonon distribution defined as $f_p^{\rm o} = [\exp(\hbar\omega/k_{\rm B}T) - 1]^{-1}$, and D_p is the phonon density of states of Al (within a harmonic approximation). Figure 11(a) shows the MD phonon conductance ($G_{t,p,{\rm MD}}$), the quantum-corrected one ($G_{t,p}$), and the phonon conductance obtained via the NEGF first-principles approach. Both the MD (top axis) and corrected temperatures are indicated in the figure.

The quantum correction of the thermal transport is generally applied to the bulk properties and is rather controversial.[68] Nevertheless, we find that the MD thermal conductance trend is very similar to the results of the NEGF approach [see Fig. 11(a)]. We attribute this agreement to the relatively small model size which results in noninteracting phonons at low temperatures. At this limit the phonon-phonon (p-p) effect not included in the NEGF approach is negligible. The MD results, which include the p-p scattering, show a slightly decreasing phonon thermal conductance at high temperatures (over 431 K, which is associated with the anharmonicity), while the NEGF results with noninteracting phonons show saturation (a plateau) at high temperatures.

Overall the phonon contribution to the thermal conductance of the biphenyl-dithiol junction is relatively small compared to the electron contribution (with the exception of the off state without the e-p interaction). Therefore, the anharmonic effect

TABLE I. Interatomic potential parameters for NEMD simulations. r, θ, and ϕ are the distance, bond angle, and torsion angle.

Interaction	Potential model	Parameters
Pair		
Al-S	$\varphi_0[\{1-\exp[-a(r-r_0)]\}^2 - 1]$	$\varphi_0 = 0.909$ eV, $a = 1.375$ Å^{-1}, $r_0 = 2.600$ Å
S-C1	$\varphi_0[\{1-\exp[-a(r-r_0)]\}^2 - 1]$	$\varphi_0 = 2.843$ eV, $a = 1.781$ Å^{-1}, $r_0 = 1.823$ Å
C1/2/3-C2 [a]	$\varphi_0[\{1-\exp[-a(r-r_0)]\}^2 - 1]$	$\varphi_0 = 8.196$ eV, $a = 1.680$ Å^{-1}, $r_0 = 1.388$Å
C3-C3	$\varphi_0[\{1-\exp[-a(r-r_0)]\}^2 - 1]$	$\varphi_0 = 7.436$ eV, $a = 1.639$ Å^{-1}, $r_0 = 1.489$ Å
Al-Al	$0.5k_r(r-r_0)^2$	$k_r = 3.989$ eV, $r_0 = 2.864$ Å
Angular		
S-C1-C2 [b]	$0.5k_\theta(\cos\theta - \cos\theta_0)^2$	$k_\theta = 3.745$ eV, $\theta_0 = 120^\circ$
C1/3-C2-C2, C2-C1/3-C2 [a]	$0.5k_\theta(\cos\theta - \cos\theta_0)^2$	$k_\theta = 11.732$ eV, $\theta_0 = 120^\circ$
C2-C3-C3 [a]	$0.5k_\theta(\cos\theta - \cos\theta_0)^2$	$k_\theta = 9.599$ eV, $\theta_0 = 120^\circ$
Torsional		
C2-C3-C3-C2	$k_\phi[1 - \cos(\phi - \phi_0)]$	$k_\phi = 2.499$ eV, $\phi_0 = 31.6^\circ$

[a]Reference 61.
[b]Reference 62.

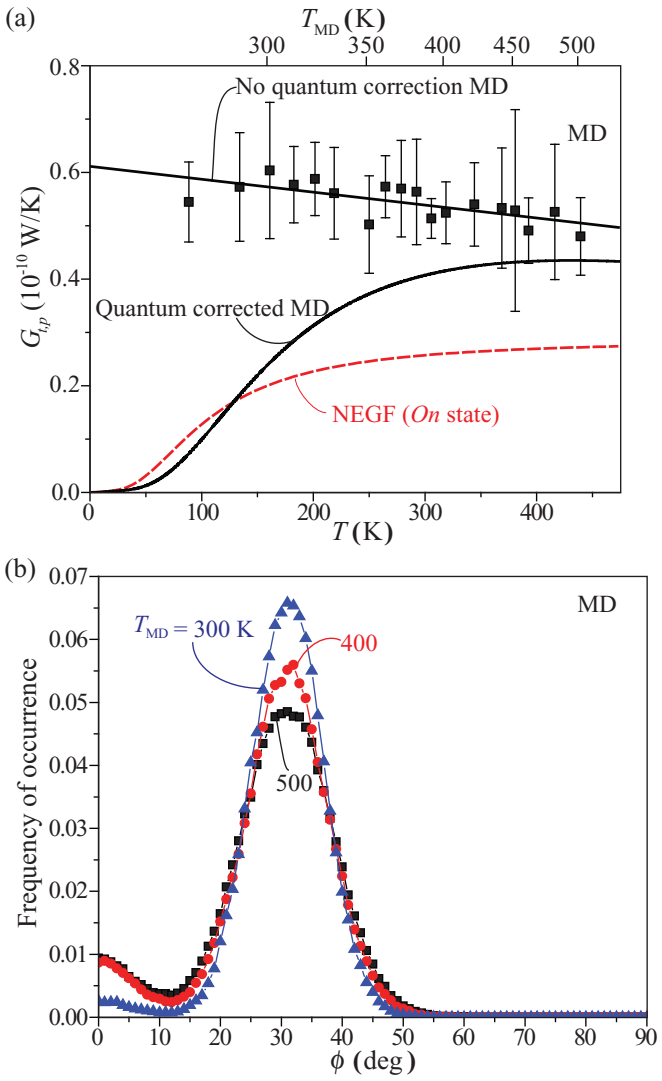

FIG. 11. (Color online) (a) Phonon thermal conductance of the biphenyl-dithiol TE junction, obtained via both the MD and NEGF calculations, versus junction temperature. (b) Frequency of occurrence of the biphenyl-dithiol molecular configurations with various torsion angles for three different values of junction temperature.

will only slightly enhance the TE figure of merit (ZT) of the junction at high temperatures.

We also use the MD calculations to analyze the torsion stability of the biphenyl-dithiol junction. In order to do so we compute the frequency of occurrence of the biphenyl-dithiol molecule with a particular torsion angle between the phenyl rings, as shown in Fig. 11(b). Clearly, the molecular geometries with the torsion angle of 30° occur most frequently. This is in agreement with the results of the conformational study within the first-principles approach discussed in the previous subsections. At higher temperatures the frequency of occurrence becomes broadened, suggesting that the molecule is likely to deviate more from the stable configuration.

IV. CONCLUSION

In summary, we present both first-principles and molecular dynamics transport calculations of the TE properties of the biphenyl-dithiol molecular junction under an applied gate voltage. Using DFT within the NEGF formalism we compute the electrical and thermal conductances, the Seebeck coefficient, and the figure of merit, taking into account the $e-p$ interactions. The results obtained demonstrate that the effect of the $e-p$ coupling on the TE properties varies with the molecular configuration. Two biphenyl-based junction configurations, one with close to planar and another with perpendicular relative orientation of the molecular phenyl rings, exhibit different responses to the inclusion of the e-p interaction into the model. The modeling illustrates the prospect of identifying molecular structural aspects that can be used to tune and eventually optimize the TE properties. Furthermore, the MD results suggest a decrease in the phonon conductance at high temperatures due to anharmonic effects.[69]

ACKNOWLEDGMENTS

This work is pursued as part of the Center for Solar and Thermal Energy Conversion, an Energy Frontier Research Center funded by the US Department of Energy, Office of Science, Office of Basic Energy Sciences under 390 Award No. DE-SC0000957.

*bdunietz@umich.edu

[1] A. Nitzan and M. A. Ratner, Science **300**, 1384 (2003).
[2] B. Xu and N. J. Tao, Science **301**, 1221 (2003).
[3] N. J. Tao, J. Mater. Chem. **5**, 3260 (2005).
[4] J. B. Neaton, K. H. Khoo, C. D. Spataru, and S. G. Louie, Comput. Phys. Commun. **169**, 1 (2005).
[5] Y. C. Chen and M. Di Ventra, Phys. Rev. Lett. **95**, 166802 (2005).
[6] Z. Huang, B. Xu, Y. Chen, M. D. Ventra, and N. J. Tao, Nano Lett. **6**, 1240 (2006).
[7] W. Zhang, N. Mingo, and T. S. Fisher, Phys. Rev. B **76**, 195429 (2007).
[8] A. Prociuk, B. V. Kuiken, and B. D. Dunietz, J. Chem. Phys. **125**, 204717 (2006).
[9] T. Perrine and B. D. Dunietz, Nanotechnology **18**, 424003 (2007).
[10] T. Perrine and B. D. Dunietz, J. Phys. Chem. A **112**, 2043 (2008).
[11] Z. Zhao and B. D. Dunietz, J. Chem. Phys. **129**, 024702 (2008).
[12] J. Tomfohr and O. F. Sankey, J. Chem. Phys. **120**, 1542 (2004).
[13] P. Reddy, S.-Y. Jang, R. A. Segalman, and A. Majumdar, Science **315**, 1568 (2007).
[14] K. Baheti, J. A. Malen, P. Doak, P. Reddy, S. Y. Jang, T. D. Tilley, A. Majumdar, and R. A. Segalman, Nano Lett. **8**, 715 (2008).
[15] J. A. Malen, P. Doak, K. Baheti, T. D. Tilley, R. A. Segalman, and A. Majumdar, Nano Lett. **9**, 1164 (2009).
[16] A. Tan, S. Sadat, and P. Reddy, Appl. Phys. Lett. **96**, 013110 (2010).
[17] M. Galperin, A. Nitzan, and M. A. Ratner, Mol. Phys. **106**, 397 (2008).

[18]K. Esfarjani, M. Zebarjadi, and Y. Kawazoe, Phys. Rev. B **73**, 085406 (2006).
[19]Y.-S. Liu, Y.-R. Chen, and Y.-C. Chen, ACS Nano **3**, 3497 (2009).
[20]T. Markussen, A.-P. Jauho, and M. Brandbyge, Phys. Rev. B **79**, 035415 (2009).
[21]Y. Dubi and M. D. Ventra, Nano Lett. **9**, 97 (2009).
[22]Y. S. Liu and Y. C. Chen, Phys. Rev. B **79**, 193101 (2009).
[23]S. H. Ke, W. Yang, S. Curtarolo, and H. U. Baranger, Nano Lett. **9**, 1011 (2009).
[24]A. Pecchia, A. D. Carlo, A. Gagliardi, T. A. Niehaus, and T. Frauenheim, J. Comput. Electron. **4**, 79 (2005).
[25]M. Galperin, M. A. Ratner, and A. Nitzan, J. Phys.: Condens. Matter **19**, 103201 (2007).
[26]T. Frederiksen, M. Brandbyge, N. Lorente, and A.-P. Jauho, Phys. Rev. Lett. **93**, 256601 (2004).
[27]N. Sergueev, D. Roubtsov, and H. Guo, Phys. Rev. Lett. **95**, 146803 (2005).
[28]N. Sergueev, A. A. Demkov, and H. Guo, Phys. Rev. B **75**, 233418 (2007).
[29]W. Ho, J. Chem. Phys. **117**, 11033 (2002).
[30]W. Wang, T. Lee, I. Kretzshmar, and M. A. Reed, Nano Lett. **4**, 643 (2004).
[31]J. I. Pascual, J. Gomez-Herrero, D. Sanchez-Portal, and H.-P. Rust, J. Chem. Phys. **117**, 9531 (2002).
[32]J. I. Pascual, N. Lorente, Z. Song, H. Conrad, and H.-P. Rust, Nature (London) **423**, 525 (2003).
[33]N. A. Pradhan, N. Liu, and W. Ho, J. Phys. Chem. B **109**, 8513 (2005).
[34]D. Segal, Phys. Rev. B **72**, 165426 (2005).
[35]K. Walczak, Physica B **392**, 173 (2007).
[36]H. Haug and A.-P. Jauho, *Quantum Kinetics in Transport and Optics of Semiconductors* (Springer, New York, 1996).
[37]M. Galperin, M. A. Ratner, and A. Nitzan, J. Chem. Phys. **121**, 11965 (2004).
[38]A. Pecchia, A. D. Carlo, A. Gagliardi, S. Sanna, and T. Fraunheim, Nano Lett. **4**, 2109 (2004).
[39]T. Frederiksen, K. J. Franke, A. Arnau, G. Schulze, J. I. Pascual, and N. Lorente, Phys. Rev. B **78**, 233401 (2008).
[40]A. M. Lunde, A. D. Martino, A. Schulz, R. Egger, and K. Flensberg, New J. Phys. **11**, 023031 (2009).
[41]E. J. McEniry, Y. Wang, D. Dundas, T. N. Todorov, L. Stella, R. P. Miranda, A. J. Fisher, A. P. Horsfield, C. P. Race, D. R. Mason, W. M. C. Foulkes, and A. P. Sutton, Eur. Phys. J. B **77**, 305 (2010).
[42]J. Taylor, H. Guo, and J. Wang, Phys. Rev. B **63**, 245407 (2001).
[43]S. Datta, Superlatt. Microstruct. **4**, 253 (2000).
[44]S. Datta, Nanotechnology **15**, S433 (2004).
[45]S. Datta, *Electronic Transport in Mesoscopic Systems* (Cambridge University Press, Cambridge, 1997).
[46]D. S. Fisher and P. A. Lee, Phys. Rev. B **23**, 6851 (1981).
[47]N. Sergueev, Ph.D. thesis, McGill University, Montreal, Canada, 2005.
[48]N. Mingo and L. Yang, Phys. Rev. B **68**, 245406 (2003).
[49]T. Yamamoto and K. Watanabe, Phys. Rev. Lett. **96**, 255503 (2006).
[50]M. P. L. Sancho, J. M. L. Sancho, J. M. L. Sancho, and J. Rubio, J. Phys. F **15**, 851 (1985).
[51]R. B. Pontes, F. D. Novaes, A. Fazzio, and A. J. R. da Silva, J. Am. Chem. Soc. **128**, 8996 (2006).
[52]J. M. Soler, E. Artacho, J. D. Gale, A. Garca, J. Junquera, P. Ordejn, and D. S nchez-Portal, J. Phys.: Condens. Matter **14**, 2745 (2002).
[53]F. Pauly, J. K. Viljas, J. C. Cuevas, and G. Schon, Phys. Rev. B **77**, 155312 (2008).
[54]A. Mishchenko, D. Vonlanthen, V. Meded, M. Burkle, C. Li, I. V. Pobelov, A. Bagrets, J. K. Viljas, F. Pauly, F. Evers, M. Mayor, and T. Wandlowski, Nano Lett. **10**, 156 (2010).
[55]L. Venkataraman, J. E. Klare, I. W. Tam, C. Nuckolls, M. S. Hybertsen, and M. L. Steigerwald, Nano Lett. **6**, 458 (2006).
[56]L. Venkataraman, J. E. Klare, C. Nuckolls, M. S. Hybertsen, and M. L. Steigerwald, Nature (London) **442**, 904 (2006).
[57]T. M. Perrine, R. G. Smith, C. Marsh, and B. D. Dunietz, J. Chem. Phys. **128**, 154706 (2008).
[58]T. M. Perrine and B. D. Dunietz, Phys. Rev. B **75**, 195319 (2007).
[59]T. M. Perrine and B. D. Dunietz, J. Am. Chem. Soc. **132**, 2914 (2010).
[60]N. Sergueev and A. A. Demkov, Phys. Rev. B **81**, 045112 (2010).
[61]B. L. Huang, A. J. H. McGaughey, and M. Kaviany, Int. J. Heat Mass Transf. **50**, 393 (2007).
[62]D. Q. Andrews, R. P. V. Duyne, and M. A. Ratner, Nano Lett. **8**, 1120 (2008).
[63]S. Shin, M. Kaviany, T. Desai, and R. Bonner, Phys. Rev. B **82**, 081302 (2010).
[64]J. Hu, X. Ruan, and Y. P. Chen, Nano Lett. **9**, 2730 (2009).
[65]M. Kaviany, *Heat Transfer Physics* (Cambridge University Press, New York, 2008).
[66]C. Z. Wang, C. T. Chan, and K. M. Ho, Phys. Rev. B **42**, 11276 (1990).
[67]J.-S. Wang, J. Wang, and J. T. Lu, Eur. Phys. J. B **62**, 381 (2008).
[68]J. E. Turney, A. J. H. McGaughey, and C. H. Amon, Phys. Rev. B **79**, 224305 (2009).
[69]T. Luo and J. R. Lloyd, Int. J. Heat Mass Transf. **63**, 1 (2010).